PASJ: Publ. Astron. Soc. Japan **60**, 951–960, 2008 October 25

Tropospheric Delay Calibrations for VERA

Mareki HONMA
Mizusawa VERA Observatory, National Astronomical Observatory of Japan, 2-21-1 Osawa, Mitaka, Tokyo 181-8588
mareki.honma@nao.ac.jp
Yoshiaki TAMURA
Mizusawa VERA Observatory, National Astronomical Observatory of Japan,
2-12 Hoshigaoka-cho, Mizusawa-ku, Oshu, Iwate 023-0861
and
Mark J. REID
Harvard-Smithsonian Center for Astrophysics, 60 Garden Street, Cambridge, MA 02138, USA

(Received 2008 February 20; accepted 2008 April 27)

Abstract

We present techniques for the tropospheric delay calibration, which is the key to increasing the accuracy of the phase-referencing astrometry with Very Long Baseline Interferometry (VLBI). We study three methods, and make a comparison of these methods to discuss the accuracy in calibration. Our results show that all three methods can calibrate the tropospheric zenith delay within accuracy of $\sim$2 cm. We also present simulations of positional errors in VLBI Exploration of Radio Astrometry (VERA) at the presence of an error in the tropospheric zenith delay, showing that parallax measurements with accuracy of 10 μas can be readily achieved for sources at high declination and with small separation angles between the target Galactic maser and extragalactic position references.

Key words: astrometry — techniques: high angular resolution — techniques: interferometric

1. Introduction

Phase-referencing VLBI (Very Long Baseline Interferometry) is a unique technique that allows one to obtain high astrometric precision for compact radio sources, such as Galactic masers. Both VLBA (Very Long Baseline Array) and VERA (VLBI Exploration of Radio Astrometry) observations of Galactic maser sources have shown that astrometry over kpc-scales is possible with phase-referencing techniques (Kurayama et al. 2005; Hachisuka et al. 2006; Xu et al. 2006; Honma et al. 2007). When phase-referencing astrometry is carried out, phase delay is the basic observable to obtain the relative positions of radio sources, and it is fundamental to precisely calibrate additional delay terms, such as those caused by errors in station coordinates, instrumental delays, tropospheric delay, ionospheric delay, and so forth.

Usually, station coordinates can be measured with an accuracy of a few mm, based on intensive monitoring of station motions by "geodetic observations" (e.g., Sovers et al. 1998). As for instrumental delays, in the case of fast-switching VLBI, the target and the reference sources are observed with the same receivers, and thus instrumental delays cancel automatically out. For VERA, where two sources are observed with two independent feeds and receivers, a horn-on-dish method is used for instrumental delay calibrations, in which artificial noise sources located on the antenna main-reflector are observed in real time to monitor the path-length difference between the two receivers (Kawaguchi et al. 2000; Honma et al. 2008). Tropospheric and ionospheric delays cannot be predicted, and thus should be calibrated by other methods. While the ionospheric contribution is dispersive and is not dominant at short cm and mm wavelengths, the tropospheric term is nondispersive, and thus its effect still exists at higher frequencies, such as the K ($\sim$22 GHz) and Q ($\sim$43 GHz) bands, which are the main observing bands of VERA.

While short-term tropospheric variations can be calibrated with simultaneous (or nearly simultaneous) phase-referencing observations of target and reference sources, there still exist long-term tropospheric delay differences (which are nearly constant or slowly varying with time). This term originates from the airmass difference between the target and the reference sources, and can be expressed as the combination of a tropospheric zenith delay and a mapping function of the troposphere. For instance, if we assume a plane parallel model for the troposphere, the tropospheric delay (in path length) can be written as

$$l = c\tau_{\rm atm}\sec Z, \tag{1}$$

where c is the speed of light, $\tau_{\rm atm}$ the tropospheric zenith delay, and Z the source zenith distance.

The tropospheric zenith delay, $\tau_{\rm atm}$, basically consists of two parts: a "dry" (or hydrostatic) part and a "wet" part (caused by water vapor). The dry part is relatively stable, and can be well modeled with surface measurements of the temperature, pressure, and elevation. A typical value for the dry component is $\sim$ 2.3 m in delay length at a sea-level site. In contrast, the wet part is problematic, since it is difficult to predict from surface weather data, and can be time variable. Its contribution is a few cm at dry sites, but can be as large as 40 cm at humid sites, such as Ogasawara and Ishigaki-jima of the VERA array, particularly during the summer. In practice, in this paper we consider path-length departures from model values, which are dominated by the wet part, but might contain small contributions from the dry component.

For phase-referencing observations, the tropospheric excess delay between two sources measured by the same antenna is given by

$$\Delta l = c\tau_{\rm atm}(\sec Z_2 - \sec Z_1) \approx c\tau_{\rm atm}\sec\bar{Z}\,\tan\bar{Z}\,\Delta Z, \quad (2)$$

where $\Delta Z = Z_2 - Z_1$ and $\bar{Z}$ represents the mean of Z_1 and Z_2. The effect of the zenith delay error on the astrometric results can be estimated through equation (2). If we consider a target-reference pair at $\bar{Z} \sim 45^\circ$ with a zenith distance difference of 1°, we then obtain $\Delta l \approx 0.024\,\tau_{\rm atm}$. Therefore, a zenith delay error of 1 cm causes a path-length difference error of 0.24 mm. This path-length error corresponds to an astrometric error of $\Delta l / B_{\rm max} \approx 22\,\mu$as, where $B_{\rm max} \approx 2300$ km is the maximum baseline of the VERA array. According to this estimate, one can see that the zenith delay offset should be calibrated at the level of 1 cm. In fact, recent simulations made by Pradel, Charlot, and Lestrade (2006) demonstrated that the error in tropspheric zenith delay can be a dominant source of error in VLBI astrometry.

Several methods have been developed to calibrate the tropospheric zenith delay in phase-referencing VLBI astrometry. Basically one can categorize these methods into two groups: (1) those with additional measurements of the troposphere independent of phase-referencing VLBI observations, and (2) those that utilize the visibility data of the target and the reference, themselves. The first category includes troposphere measurements with GPS (Global Positioning System) receivers, geodetic-mode VLBI observations (Reid & Brunthaler 2004), or water vapor radiometers (e.g., Roy et al. 2006); the second category includes the phase-fitting method (Brunthaler et al. 2005) or image optimization (which is newly proposed here). Pioneering studies reported on zenith delay calibrations with an accuracy of a few cm or smaller, and played major roles in phase-referencing VLBI astrometry (e.g., Reid & Brunthaler 2004; Xu et al. 2006). However, these studies were made with the VLBA, whose stations are located at rather dry sites. On the other hand, the VERA stations are located in humid areas, in particular at two stations on islands in the Pacific ocean (Ogasawara and Ishigaki-jima). In order to see how precisely the tropospheric delay can be calibrated for the VERA array, we have conducted experiments to compare the calibration methods available for VERA (GPS, geodetic-mode VLBI, and image optimization). Here, we present the results of detailed comparisons and a discussion of the effects on the astrometric accuracy of VERA.

2. Methods

In this section, we briefly summarize the three calibration methods (GPS, geodetic-mode, and image-optimization) considered in the present paper.

2.1. GPS

The basic idea of a tropospheric measurement with GPS data is similar to geodetic-mode VLBI (which will be described in the next subsection), in the sense that the observed delays of radio sources whose positions are accurately known (GPS satellites/extragalactic AGNs) are used to measure the tropospheric delay. In normal GPS observations (i.e., measuring station positions), signals from multiple (usually more than four) GPS satellites are received at each station, and the delays of the L1/L2 signals are used to solve the station positions. For tropospheric measurements, station positions are regarded as known parameters (and thus fixed), and delay residuals are used to solve for the tropospheric zenith delays by assuming a tropospheric mapping function. Thus, prior to the tropospheric delay measurements, accurate positions of the GPS receiving stations must be determined; this can also be done with long-term observations of GPS satellites. Note that the effect of the (dispersive) ionosphere is usually corrected for based on multifrequency observations in the L1/L2 bands.

For a tropospheric calibration in VERA, continuous GPS observations have been carried out at all four stations to monitor the time variation of tropospheric zenith delays. The GPS receiving antenna is mounted on the roof of the telescope-control building at each station, which is ~ 50 m away from the telescope, itself. Trimble NetRS receivers and choke-ring antennas are used. The sampling rate and elevation mask are 30 s and 10°, respectively. External frequency standards (hydrogen masers) are used to keep accurate sample timing and to reduce clock ambiguities in the observations. In the analysis, the GIPSY-OASIS II (release 4) software developed by NASA/JPL is used, and a precise point processing method (PPP method: Zumberge et al. 1997) is applied. The three-dimensional coordinates of each station are solved daily, and the wet zenith delay is estimated at 5 min intervals. In modeling the troposphere, Niell's mapping function (Niell 1996) is used.

In general, there is a strong correlation between the vertical component of the antenna coordinates and the zenith delay estimates. The solutions to the zenith delay become unstable if one requires solutions with time resolutions that are too high. To resolve this conflict, GIPSY-OASIS II adopts a stochastic random-walk model for estimating parameters that vary rapidly, like the wet zenith delay. The accuracy of the wet zenith delay, estimated from GPS data, has been investigated by several authors by comparing with radiosonde data, water vapor radiometers, and/or numerical weather analysis data (e.g., Iwabuchi et al. 2000). The rms error in the wet zenith delay is estimated to be ~ 1.5 cm in the Japanese region.

2.2. Geodetic-Mode Observations

In geodetic-mode observations, bright sources with accurately known positions are observed successively with a typical on-source time of 1 min. The basic idea of this method is the same as that in geodetic VLBI experiments, which aim at precise measurements of station coordinates by using geometric delays of radio sources between stations. In contrast to normal geodetic VLBI, in geodetic-mode observations, the station coordinates are already known, and the geometric delays of radio sources are used to find a solution to the tropospheric zenith delay at each station. To seek a solution to the station-based tropospheric zenith delay, it is essential to observe low-elevation-angle sources, so that *differences* in $\sec Z$ term among stations become significant. Thus, only bright sources can be used for this kind of observation so as to ensure detections at low elevation angles, where atmospheric

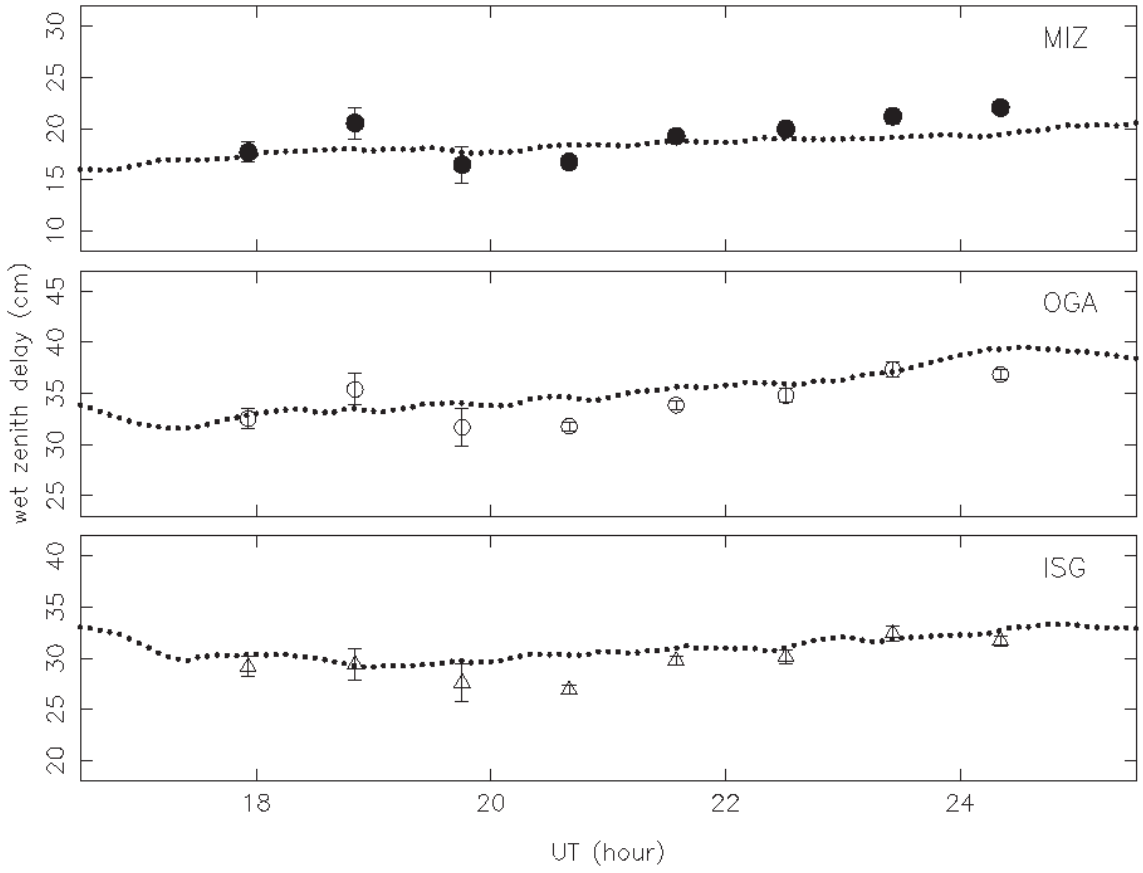

Fig. 1. Wet components of the tropospheric zenith delay measured at VERA stations on DOY (the day of the year) 207 of 2007 with GPS (dotted lines) and geodetic-mode VLBI observations (markers with error bars), for the Mizusawa, Ogasawara, and Ishigaki-jima stations (from top to bottom).

attenuation can be significant. In practice, 20–30 bright ICRF (International Celestial Reference Frame) sources, with positional accuracy within 1 mas, are observed within a 30–45 min period to obtain a zenith delay offset (and sometimes a zenith delay rate). Since the observed delay residual of each source consists of a tropospheric delay term as well as a clock offset, we solved both the zenith delay and the clock offsets simultaneously. When solving the zenith delay with geodetic-mode observations, we used the mapping function derived in Thompson, Moran, and Swenson (2001), which includes the higher-order corrections to the simple sec Z mapping function. Since the minimum elevation angle is above 10° for geodetic-mode observations, there is no significant difference, even when a more sophisticated mapping function (such as Niell's mapping function) is considered. We note that geodetic-mode observations have been routinely used in phase-reference VLBA observations, and have resulted in the zenith delay calibration at the level of 1 cm (e.g., Reid & Brunthaler 2004).

2.3. *Image-Optimization*

In the image-optimization technique, many trial phase-referenced maps are produced by varying the zenith delay at each station to find the best image, judged from the peak brightness in the map. The basic idea is that a zenith delay offset causes errors of visibility phase, which degrade the coherence of phase-referenced maps. Thus, finding an image with the greatest peak brightness can provide good estimates of the zenith delay at each station. In practice, trial values of the tropospheric zenith delay (typically ranging between plus and minus 10 cm of an initial estimate, at intervals of 0.5 to 1 cm) are chosen, and the visibility phases are shifted accordingly. Then, the visibility data are Fourier-transformed to make synthesized images, and the peak brightness is measured. The behavior of the peak brightness against the zenith delay offset is usually simple, having a single peak at the optimum value of the zenith delay.

Strictly speaking, this problem should be solved simultaneously in 4-dimensions (zenith delays for 4 stations of the VERA array), but this cannot be done practically, since it would be extremely time consuming (e.g., if we have 10 trial values of the zenith delay for each station, the full 4-dimensional solutions for the VERA array would require 10^4 phase-referenced maps). Instead of 4-dimensional solutions, here we conduct 1-dimensional solutions for each station, while varying the zenith delay at one station and not changing the zenith delays at the other stations. We perform such a 1-dimensional search for each of four stations and then continue the process (four 1-dimensional searches) iteratively until the solutions converge. According to our experience, this method works fairly well, and in most cases solutions converge

after 2 or 3 iterations. Practically, we use this method to recalibrate the phase-referenced visibilities after the calibration of the tropospheric zenith delay with GPS to check if there are any remaining zenith delay residual.

We note that the image-optimization method is similar to the phase fitting (Brunthaler et al. 2005), in a sense that both methods utilize the phase-referenced visibilities, themselves, rather than obtaining additional calibration data (such as GPS and geodetic-mode observations). However, the main difference between the two methods is that, while phase fitting can be applied only to bright sources for which phase can be obtained within sufficiently short time (such as a few to ten min), image optimization can generally be applied to weak sources that can only be detected in the phase-referenced map after integrating for hours.

3. Comparisons between the Methods

3.1. GPS versus Geodetic-Mode

In order to compare two tropospheric zenith delays measured by GPS and geodetic-mode observations, we conducted two test runs of geodetic-mode observations with VERA. The VERA observations were made on the day of the year (DOY) 207 and 213 of 2007 (2007 July 26 and August 1). Each observation lasted for 8 hr, during which 30 min blocks of geodetic-mode observations were made continuously. For the run on DOY 207, the Iriki station failed. For the run on DOY 213, all four stations participated, but the fringe detection rate was lower than that on DOY 207, chiefly due to bad weather and thus high system temperatures. In both experiments, the observing frequency was centered at 22.2 GHz and the total spanned bandwidth was 464 MHz, obtained from fifteen 16 MHz IF channels spaced by 32 MHz. On-source integration time was set to 1 min, and in each 30 min block ~ 20 sources were observed.

Figure 1 shows the wet zenith delay for DOY 207 (after subtracting a constant hydrostatic delay), measured by GPS and geodetic-mode observations. GPS zenith delays were obtained every 5 min, while geodetic-mode solutions were obtained approximately hourly by fitting the data over 55 min segments. The results are shown for the three stations that participated in the experiment, namely, Mizusawa (MIZ), Ogasawara (OGA), and Ishigaki-jima (ISG). For geodetic-mode measurements, formal $1\,\sigma$ error bars ($\sigma_{\rm GEO}$) are also plotted. Since the observations were made in the middle of the summer (July 26), the wet zenith delay was large, upward of 40 cm. These are typical values of the wet zenith delay, especially for island stations such as Ogasawara and Ishigaki-jima. Nevertheless, as can be seen in figure 1, both GPS and geodetic-mode observations are consistent in value of the zenith delay, with typical differences of less than a few cm. Note that the three stations show a trend of a rising wet delay with time. This is probably related to a gradual change in the weather over a scale of 1000's km. However, for the observations on DOY 213, this kind of trend was not seen.

Figure 2 shows the distribution of differences in zenith delay between GPS and geodetic-mode observations (GPS−GEO) for two days' data, which yielded 52 measurements. Basically, there is no systematic difference between GPS and geodetic-mode zenith delays, with the average difference between the two techniques of 0.24 ± 0.50 cm with a standard deviation of 3.6 cm. Here, the error of the mean is obtained as a $1\,\sigma$ standard error of the mean. This shows that both methods can trace the wet zenith delay without any systematic offset.

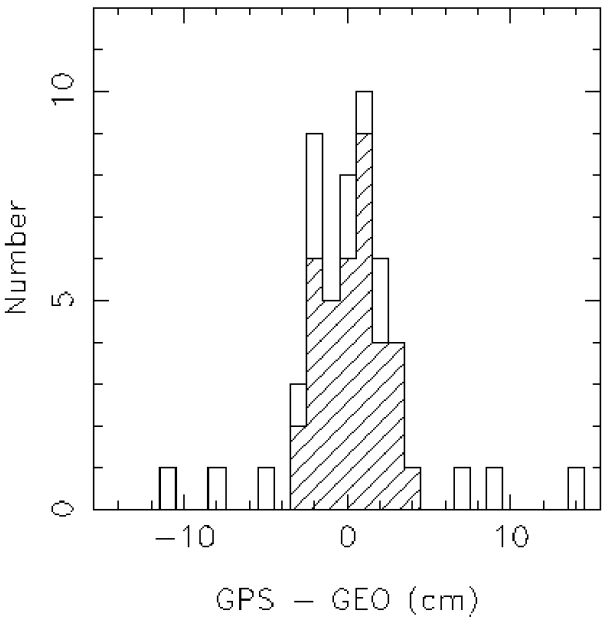

Fig. 2. Distribution of the difference in zenith delay between GPS and geodetic-mode observations, obtained on DOY 207 and DOY 213 in 2007 with VERA. The shadowed area shows relatively good data for geodetic-mode observations ($\sigma_{\rm GEO} \leq 1$ cm) .

The standard deviation of $\sigma_{\rm GPS-GEO} = 3.6$ cm is dominated by a small number of uncertain ($\sigma_{\rm GEO}$ of 3–5 cm) data in the geodetic-mode observations (owing to chiefly bad weather and thus high system temperatures). If we conservatively use only the geodetic-mode results with $\sigma_{\rm GEO} < 1$ cm, the standard deviation of GPS−GEO estimates decreases to 1.8 cm (the mean of the difference is 0.27 ± 0.30 cm). This is likely to represent a typical value of the standard deviation of GPS−GEO data (the distribution of GPS−GEO for $\sigma_{\rm GEO} \leq 1$ cm is shown in figure 2 as shadowed area). Assuming that the GPS data has $\sigma_{\rm GPS} = 1.5$ cm, this suggests that the geodetic-mode zenith delays indeed have uncertainties of 1.0 cm.

3.2. Image-Optimization versus Geodetic-Mode

In order to compare the image-optimization (IOP) results with the geodetic-mode ones, we used the VLBA data for Sgr A* of Reid and Brunthaler (2004). We note that currently tropospheric calibrations with geodetic-mode observations are not regularly done in VERA's astrometric observations, and thus here we used the VLBA data to check the validity of the image-optimization technique. In total 7 epochs were available for geodetic-mode calibrations, including 4 epochs in 2003 April and May and 3 epochs in 2007 April. At each epoch, 3 geodetic-mode observations lasting for 45 min were carried out at the beginning, in the middle, and at the end of 7 hr observing sessions. Each geodetic-mode block was independently used to determine the zenith delay and the zenith delay

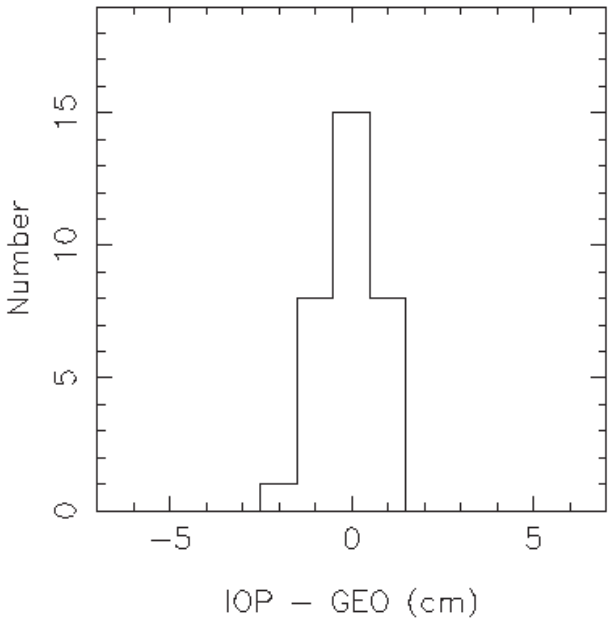

Fig. 3. Distribution of the difference in zenith delay between image-optimization and geodetic-mode observations, obtained for Sgr A* data observed with VLBA.

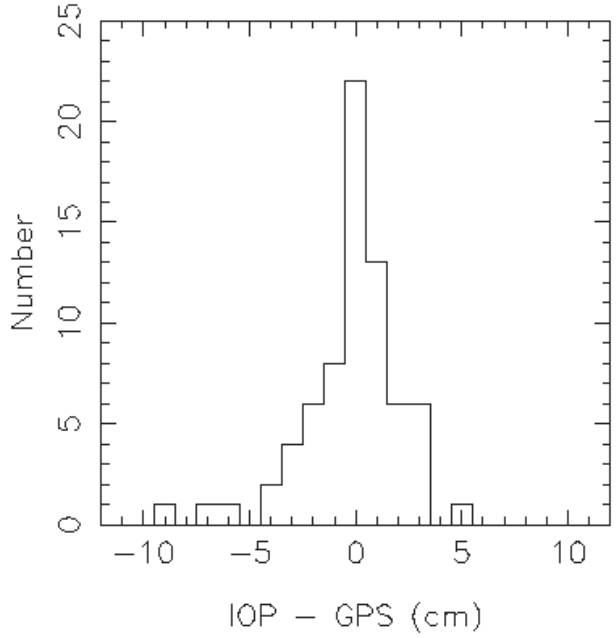

Fig. 4. Distribution of the difference in zenith delay between image-optimization and GPS obtained for 18-epoch VERA observations of W 49N and S 269.

rate, and linear interpolations were made to calibrate the visibility of Sgr A*. The use of typically 8–10 VLBA stations, which provides a larger number of baselines and larger differences in elevation angle among stations than those of VERA, yields formal errors for zenith delays that usually are less than 1 cm (e.g., Brunthaler et al. 2005).

We applied the image-optimization to the visibility of J1745−283, which had been phase-referenced to Sgr A*. Since the visibilities were initially calibrated for the tropospheric zenith delay by geodetic-mode observations, the application of image-optimization to these data allowed a comparison of the two methods. Using image-optimization, we determined the zenith delay residuals for 5 stations (namely, Pie Town, Fort Davis, Kitt Peak, Los Alamos, and Owens Valley). For other antennas that provide longer baselines, Sgr A* was not detected due to the strong interstellar scattering (Reid & Brunthaler 2004), and zenith delays could not be determined for these antennas. From the 7 epochs with 4–5 antennas, we obtained 32 image-optimization solutions for zenith delay residuals. Figure 3 shows the distribution of the zenith delay residuals obtained by image-optimization. The distribution again peaks near zero, with a mean of IOP−GEO of -0.27 ± 0.14 cm. This indicates that there is no systematic offset between geodetic-mode and image-optimization calibrations. The standard deviation of the difference in zenith delay was 0.8 cm, which is smaller by a factor of ~ 2 than $\sigma_{\mathrm{GPS-GEO}}$.

3.3. Image-Optimization versus GPS

In order to compare the performances of image-optimization and GPS techniques, we applied the image-optimization technique to VERA data that were initially calibrated for the tropospheric zenith delay using the GPS technique. We used the multiepoch data for S 269 (Honma et al. 2007) and also for W 49N, whose astrometric results will be published elsewhere. In total, we analyzed 18 epochs of observations conducted with the full 4-station array of VERA. For all data, fringes were found for the position-reference sources (J0613+1306 for S 269 and J1905+0952 for W 49N), phase-referenced visibilities were produced for the maser sources, and then the image optimization was conducted. Figure 4 shows the distribution of the zenith delay residuals obtained by the image optimization. Again, the distribution sharply peaks at zero, with a mean of 0.01 ± 0.37 cm, and a standard deviation of 3.1 cm.

Note that there are some cases in which the residual is relatively large, and exceeds 5 cm. In the worst case, there is one measurement indicating a residual of 18 cm, which was obtained for Ishigaki-jima at a summer season (DOY 135 of 2005). The exact reason for this large discrepancy is unknown, but it is possibly due to calibration errors in GPS, most likely an error in the ionospheric correction. (According to our experience of station-position measurements with GPS, we found large GPS uncertainties when one of the L1/L2 signals weakened due to receiver-system trouble; a lack of one frequency severely degrades the ionosphere calibration.) If we exclude 2 outliers with IOP−GPS that is larger than 8 cm, we obtain a mean of IOP−GPS as -0.12 ± 0.25 cm and a standard deviation of 2.1 cm for 70 independent measurements. Thus, the image-optimization and GPS techniques agree with each other at the level of 2 cm, being similar to that of GEO−GPS.

3.4. Comparison of Three Methods

A summary of the three comparisons is listed in table 1. The comparisons between GPS, geodetic-mode, and image-optimization calibrations indicate that there are no systematic offsets among these techniques, and that the zenith delay can be

Table 1. Summary of comparisons of three methods.

Comparison	Number of data	Mean (cm)	σ (cm)
GPS−GEO*	37	0.27 ± 0.30	1.8
IOP−GEO	32	-0.27 ± 0.14	0.8
IOP−GPS†	70	-0.12 ± 0.25	2.1

* Using the geodetic-mode results with a formal error less than 1 cm.
† Excluding two extreme cases in which IOP−GPS is greater than 8 cm at Ishigaki-jima station.

calibrated to 1–2 cm by each technique. The smaller standard deviation for IOP−GEO than that for GPS−GEO or IOP−GPS may indicate that GPS estimates are marginally worse than the others; perhaps the values of σ are dominated by errors in the GPS measurements. We note, however, that we obtained the IOP−GEO distribution using VLBA data, where the site conditions (i.e., humidity) are better than those of VERA, and this could explain the smaller value of $\sigma_{\mathrm{IOP-GEO}}$ than that of $\sigma_{\mathrm{GPS-GEO}}$ or $\sigma_{\mathrm{IOP-GPS}}$, which were obtained with the VERA stations.

4. Effects of Zenith Delay Residual on Astrometry

In previous sections, we have shown that the tropospheric zenith delay can be calibrated at the level of 1–2 cm through the methods described above. Here, we discuss how the astrometric results of VERA would be affected by the zenith delay residuals. As discussed in previous studies (e.g., Pradel et al. 2006; Asaki et al. 2007), it is not easy to estimate the astrometric errors in phase-referencing VLBI analytically, and simulations are required. Here, to calculate an astrometric error caused by zenith delay errors, we simulated phase-referenced visibilities for the VERA array with independent zenith delay errors at each station. For the sake of simplicity, we assumed that the source was pointlike (no structure) and the visibilities have no thermal noise (i.e., infinitely large S/N ratio). By Fourier transforming the simulated visibilities, maps were created and shifts of the brightness peak position were measured with respect to the map without zenith delay errors.

4.1. Astrometric Error Due to Zenith Delay Offset

Figure 5 show the results of simulations for 3 cases of source declinations, $\delta = -30°$, $+15°$, and $+60°$, with a target–calibrator separation angle (SA) of 1°. We assumed that the sources were fully tracked when they were above a minimum elevation angle, EL_{min}. The values of EL_{min} were set to be $+15°$ for $\delta = -30°$, $+20°$ for $\delta = +15°$, and $+30°$ for $\delta = +60°$, which are practical values for real VERA observations. We plot the position offsets due to the presence of a zenith delay error of 1 cm at one station, while varying the position angle (PA), measured from north through east, of the calibrator with respect to the target on the sky plane. Note that in the simulations considered here, a zenith delay offset of 1 cm is added only to one station, and no offset to three other stations.

The position offsets in figure 5 show sinusoidal variations with PA, with amplitudes heavily dependent on the target declination. For the $\delta = -30°$ case (appropriate for Galaxy center sources), the position offsets due to a zenith delay residual of 1 cm are as much as 0.1 mas for $X \equiv \Delta\alpha \cos\delta$ and 0.2 mas for $Y \equiv \Delta\delta$, where α and δ are right ascension and declination of the target. Thus, for a low declination source, such as Sgr A*, the zenith delay residual is a serious problem of parallax measurements. We note that this is also the case with Sgr A* astrometry with VLBA. Due to interstellar scattering, Sgr A* is resolved with baselines longer than ~ 2000 km, and hence the effective array size of VLBA for Sgr A* is simillar to that of VERA. Since the astrometric error can be roughly estimated as $\Delta l / B_{\mathrm{max}}$ (where Δl is the path length error and B_{max} is the maximum baseline length), it is expected that Sgr A* observations with VLBA provide the same astrometric accuracy as those simulated here for the VERA array do. In fact, Reid and Brunthaler (2004) used the geodetic-mode observations to calibrate the zenith delays in their Sgr A* astrometry with VLBA, and even after calibrating the zenith delay at the level of 1 cm, they were still unable to detect the parallax due to an east–west direction scatter of 0.05 to 0.1 mas, which is comparable to the expected value of the Sgr A* parallax (0.125 mas for 8 kpc distance). Their results are consistent with our simulation ones if one considers that separation angles between Sgr A* and calibrators are $\sim 0.^{\circ}7$.

In figure 5, one can also see that the effect of the zenith delay on astrometry decreases dramatically with increase in source declination. This is of course due to the fact that a higher elevation angle makes $\sec Z$ term smaller. For instance, in the case of $\delta = +15°$, a zenith delay residual of 1 cm causes an astrometric error of $\sim 20\,\mu$as for X and $\sim 30\,\mu$as for Y, smaller by a factor of ~ 5 than those for $\delta = -30°$. Thus, above $\delta = +15°$, one can expect that the astrometric error caused by a zenith delay offset of 1 cm is typically less than $\sim 30\,\mu$as. However, one should note that the simulations present an astrometric offset caused by a zenith delay offset at only one station. In practice, each station should have a different zenith delay offset, and a real astrometric error would be determined by the combinations of the zenith delay offsets at all 4 stations, which could in some cases partially cancel out or reinforce each other (see discussion in subsection 4.3).

4.2. Linearity of the Results

In the previous subsection, we presented simulation results for a pair of sources with SA of 1° and a zenith delay offset of 1 cm. To extrapolate these results to more general cases (of different values of SA and zenith delay offset), here we check the dependence of the position offsets on SA and the zenith delay offset. If the position shift is much smaller compared to the interferometer beam size, one expects that this small perturbation would scale linearly with SA and zenith delay offset. In order to check this, we simulated data with varying values of SA and zenith delay offset. Figure 6 shows the resulting position offset versus the zenith delay offset (from 1 to 3 cm) for 4 stations (with $\delta = -30°$, SA $= 1°$, and PA $= 0°$). We note that here, in the same manner as described in figure 5, a zenith delay offset is added only to one station, and no offset is added to the three other stations. In figure 6, the best-fit lines for each station are also shown, demonstrating that the position offsets indeed scale linearly with the zenith delay offsets. Figure 7

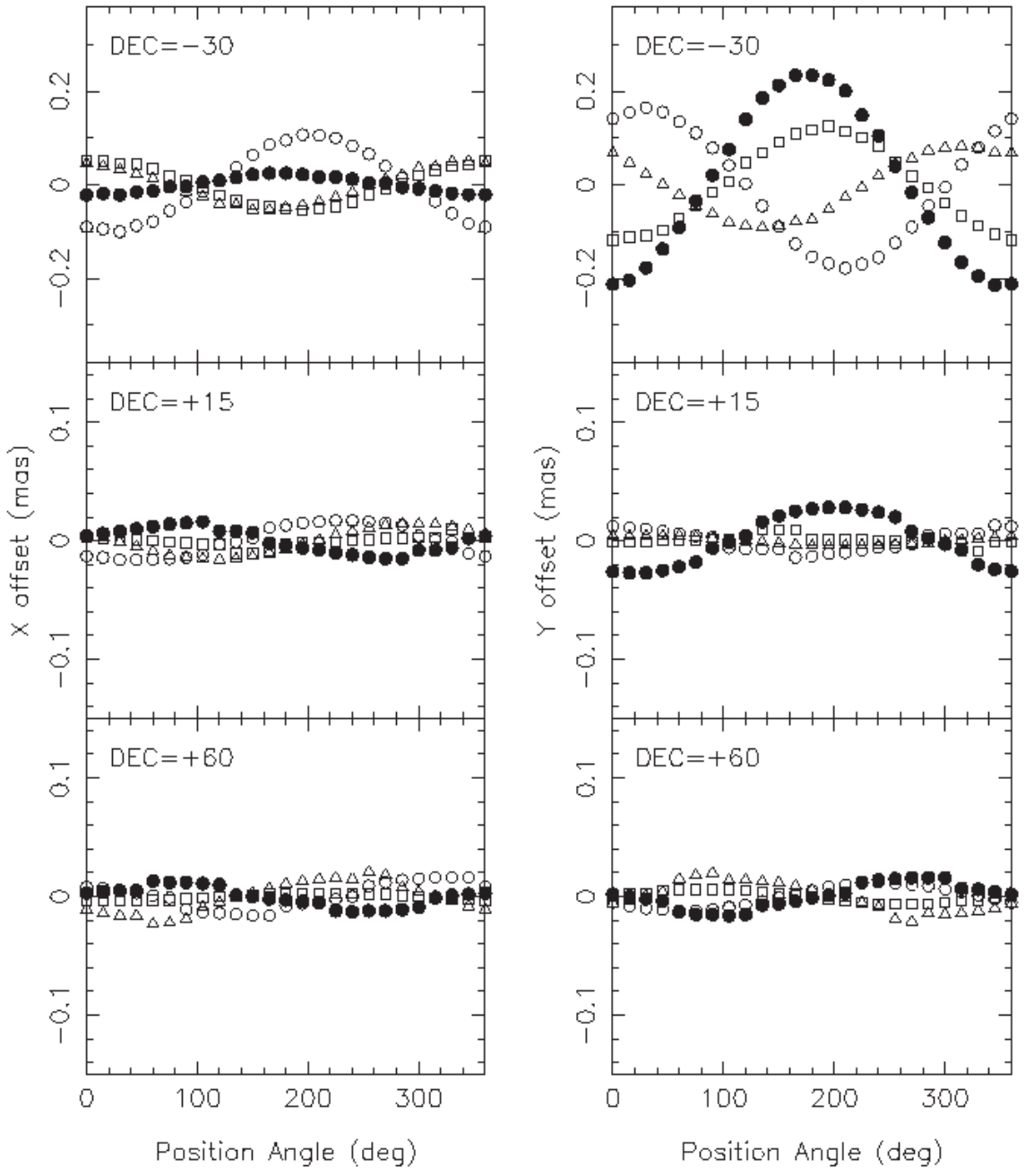

Fig. 5. Simulated position changes caused by a zenith delay error of 1 cm at each station, plotted against the position angle (PA) on the sky from the target to the reference source. Filled circle: Mizusawa, square: Iriki, open circle: Ogasawara, and triangle: Ishigaki-jima. PA = 0° is for a reference source to the north and 90° to the east of the target. Note that we added a zenith delay offset of 1 cm only to one station and 0 cm to the three other stations. Left panels are for right ascension offsets ($X = \Delta\alpha \cos\delta$) and right panels for declination offsets ($Y = \Delta\delta$). Top panels are for the source declination of $\delta = -30°$, middle for $\delta = +15°$, and bottom for $\delta = +60°$.

provides similar plots for the position offset versus SA (with $\delta = -30°$, zenith delay offset = 1 cm, and PA = 0°), and again, the results scale linearly with SA. Therefore, one can safely assume that linear extrapolation of our results in figure 5 truly reflects the general behavior of the position shifts under various conditions.

4.3. Monte Carlo Simulations

The simulation results in the previous subsections provide a reasonable estimate of the effect of the zenith delay offset at each station on the astrometric results. However, in practical radio observations, each station has a different value of zenith delay offset, and thus the final astrometric results would be determined by the combination of zenith delay offsets at the 4 VERA stations. Also, the zenith delay offsets vary from

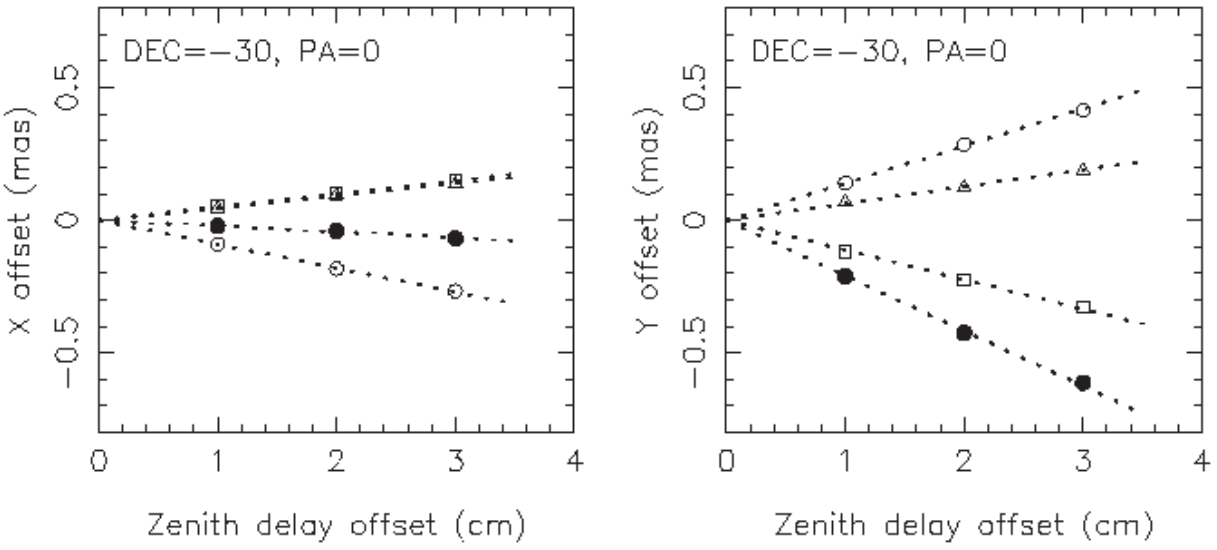

Fig. 6. Simulated position shift with varying zenith delay error at each station (filled circle: Mizusawa, square: Iriki, open circle: Ogasawara, and triangle: Ishigaki-jima). Here, the source declination, the position angle, and the separation angle are fixed to be $\delta = -30°$, PA $= 0°$, and SA $= 1°$. The dotted lines are best-fits to the data, showing that the position shift dependence on the zenith delay is linear.

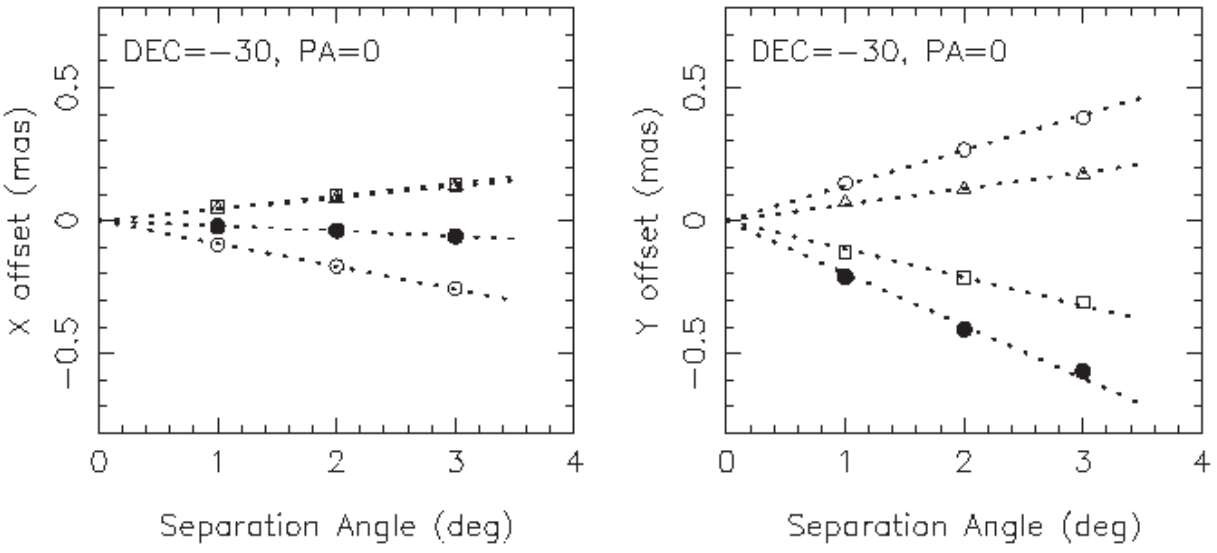

Fig. 7. Simulated position shift with varying separation angle for the pair (filled circle: Mizusawa, square: Iriki, open circle: Ogasawara, and triangle: Ishigaki-jima). Here, the source declination, the position angle, and the zenith delay error are fixed to be $\delta = -30°$, PA $= 0°$, and $\tau_{\rm atm} = 1$ cm. The dotted lines are best-fits to the data, showing that the position shift dependence on the pair separation angle is also linear.

epoch to epoch, which adds random noise to final astrometric solutions such as parallax and proper motions. In order to simulate the astrometric error in practical radio observations, we have conducted Monte Carlo simulations. We assumed that the zenith delay offset at each station follows a normal distribution (i.e., Gaussian) with a standard deviation of $\sigma = 1$ cm and a mean of 0 cm. We also assumed that the zenith delay offsets at all stations are uncorrelated, and that the astrometric results can be obtained by a linear summation of contributions from each station's zenith delay offset (this assumption was in fact confirmed to be valid by using our simulation code). We considered six representative cases, with three source declinations of $\delta = -30°$, $+15°$, and $+60°$, and with two target–calibrator PAs of 0° and 90°. In all cases, 10^5 simulations were made, with a fixed value of SA of 1°, and then the standard deviations of the position shifts were obtained as $\sigma_X = [\sum (X - \bar{X})^2/N]^{1/2}$, and in the same manner for Y (note that $\bar{X}$ and $\bar{Y}$ are practically 0 here, because we assumed a normal distribution with a mean of 0).

Table 2 summarizes our results in the six cases. Since a typical error in the zenith delay measurements was ~ 2 cm for VERA, the numbers in table 2 should be doubled for discussing practical VERA observations. For low declination sources (e.g., $\delta = -30°$ such as Sgr A*), a 2 cm zenith delay yields poor astrometric results, with σ_X and/or σ_Y exceeding 0.1 mas. On the other hand, for a declination higher than $+15°$, the

Table 2. Summary of Monte Carlo simulations.*

Declination	PA	σ_X (mas)	σ_Y (mas)
−30°	0°	0.116	0.226
−30°	90°	0.042	0.104
+15°	0°	0.016	0.029
+15°	90°	0.025	0.008
+60°	0°	0.015	0.009
+60°	90°	0.025	0.028

* All above results assume SA = 1° and 1 cm standard deviation for zenith delay offset at each station.

astrometric errors are typically 50 μas or less, and in some cases at most 20–30 μas. Therefore, even for zenith delay offsets at the level of 2 cm, an astrometric precision of a few tens of μas is achievable. We note that this is a position uncertainty for a single epoch measurement, and parallax uncertainty derived from measurements at many epochs will be less (see section 5). We also note that in this subsection we assume SA of 1°. For target–calibrator separations of 2.°2, which is the largest dual-beam separation angle for the VERA system, the astrometric accuracy in table 2 could be degraded by a factor of 4.4 (a factor of 2 from zenith delay of 2 cm and 2.2 from beam separation angle).

5. Discussion

VERA's goal is to attain 10-μas-level accuracy for parallax measurements (as well as proper motions) of Galactic maser sources. As shown in the previous section, zenith delay errors with $\sigma \sim 2$ cm lead to astrometric errors that are somewhat larger than the target accuracy for SA = 1°. However, for a high-declination source (i.e., $\delta > +15°$), 10-μas-level accuracy can be achieved with a reduction of the uncertainty by a factor of a few.

This reduction can be simply achieved by increasing the number of observations, since wet zenith delay errors are largely uncorrelated over only a few days. For instance, suppose that we observe a source every six months (at the maximum projected elongation of the Earth's orbit) for 1.5 yr. This set of observations contains $N = 4$ independent measurements, and thus the expected parallax uncertainty should be reduced by a factor of $\sqrt{N-1} = 1.7$, compared to the single-epoch uncertainty (shown in table 2). Usually, with VERA, target stars are monitored every one or two months, and thus N is often as large as 10, resulting in parallax uncertainty reduction by a factor of 3 relative to the single-epoch values in table 2. For some important sources (such as Sgr A* or W 49), it is worth trying to increase N significantly, although this cannot be done for a large number of sources, owing to limited telescope time.

For some good source configurations (e.g., $\delta > +15$ and/or SA < 1°), the reduction by a factor of 2–3 provides a parallax accuracy of 10 μas (or even higher). This indicates that VERA's target accuracy can be achievable with the current calibration methods described in this paper, as long as the tropospheric delay is the dominating source of astrometric error. In fact, Honma et al. (2007) reported a high-precision parallax measurement for S 269 (189 ± 8 μas) against the reference J0613+1306. The S 269 pair has SA = 0.°7, $\delta = +13°$, and PA = 192°, which should be compared to the third case in table 2 (i.e., north–south pair). When SA = 0.°7 is considered, the expected single-epoch astrometric error is $\sigma_x = 0.022$ μas, which is quite close to the measured value, based on the scatter in post-fit residuals, of $\sigma_x = 0.025$ μas. Thus, the results obtained here are consistent with real observations.

On the other hand, challenging sources (e.g., low declination and/or large separation angle) require further improvements in the zenith delay calibrations to achieve VERA's target accuracy. For instance, for sources with SA of 2° (note that 2.°2 is maximum limit for VERA's dual beam), the astrometric uncertainty will be doubled from the values given in table 2, and a zenith delay calibration with $\sigma \sim 1$ cm would be required to achieve VERA's target accuracy. One way to improve the atmospheric calibration is to carefully select observing dates for less-humid weather. For instance, a source toward RA = 18 h has a right ascension parallax peak around March 20 and September 20. Because the parallax curve is sinusoidal with 1 yr period, the parallax amplitude remains 93% of its maximum at two weeks before and after the peak date, allowing near optimum observations at the end of August or in early October. Such dates provide dramatically different observing conditions; it is generally very humid at the end of August with a zenith delays of ~ 40 cm at Ishigaki-jima and Ogasawara, whereas in the middle of October one can expect only ~ 20 cm of wet zenith delay. Thus, one should carefully choose observation dates to reduce the total wet zenith delay. Finally, we note that new calibration techniques, such as bi-gradient phase referencing using multiple pairs (Doi et al. 2006), may be able to reduce the zenith delay uncertainty even further.

6. Summary

We compared three methods to remove tropospheric delay errors, which is the key calibration used to achieve high position accuracy with phase-referencing VLBI. Our results have shown that zenith delays obtained with GPS, geodetic-mode, and image-optimization techniques agree with each other with an rms zenith path length difference of between 1 and 2 cm. No systematic offsets were found between the methods. According to our simulation of VERA's position accuracy, parallax measurements with 10–20 μas uncertainty can be readily done for reasonably well-situated sources (i.e., $\delta > 15°$ and SA < 1°), even in the presence of 2 cm errors in the zenith delay. For sources with lower δ and/or larger SA, the effect of a zenith delay error becomes more serious, and better calibrations will be needed to reach the target accuracy of VERA.

References

Asaki, Y., et al. 2007, PASJ, 59, 397
Brunthaler, A., Reid, M. J., Falcke, H., 2005, ASP Conf. Ser., 340, 455
Doi, A., et al. 2006, PASJ, 58, 777
Hachisuka, K., et al. 2006, ApJ, 645, 337
Honma, M., et al. 2007, PASJ, 59, 889
Honma, M., et al. 2008, PASJ, 60, 935
Iwabuchi, T., Naito, I., & Mannoji, N. 2000, J. Geophys. Res., 105, 4573
Kawaguchi, N., Sasao, T., & Manabe, S. 2000, Proc. SPIE, 4015, 544
Kurayama, T., Sasao, T., & Kobayashi, H. 2005, ApJ, 627, L49
Niell, A. E. 1996, J. Geophys. Res., 101, 3227
Pradel, N., Charlot, P., & Lestrade, J.-F. 2006, A&A, 452, 1099
Reid, M. J., & Brunthaler, A. 2004, ApJ, 616, 872
Roy, A. L., Rottmann, H., Teuber, U., & Keller, R. 2007, in Proc. 8th European VLBI Network Symposium, ed. A. Marecki et al., 58
Sovers, O. J., Fanselow, J. L., & Jacobs, C. S. 1998, Rev. Mod. Phys., 70, 1393
Thompson, A. R., Moran, J. M., & Swenson, G. W., Jr. 2001, Interferometry and Synthesis in Radio Astronomy, 2nd ed. (New York: John Wiley & Sons), chap. 9
Xu, Y., Reid, M. J., Zheng, X. W., & Menten, K. M. 2006, Science, 311, 54
Zumberge, J. F., Heflin, M. B., Jefferson, D. C., Watkins, M. M., & Webb, F. H. 1997, J. Geophys. Res., 102, 5005